

RESEARCH ARTICLE

Open Access



# Recurrence intervals for $M > 7$ Miyagi-ken-Oki earthquakes during an $M \sim 9$ earthquake cycle

Ryoko Nakata<sup>1\*</sup> , Naoki Uchida<sup>2,3</sup>, Takane Hori<sup>4</sup> and Ryota Hino<sup>2</sup>

## Abstract

The 2011 Tohoku-Oki great earthquake increased the difficulty of evaluating the long-term probability of seismic activity along the Japan Trench because of the unknown impact of the unprecedentedly large slip. In this study, the long-term activity of “Miyagi-ken-Oki earthquakes”, an  $M > 7$  earthquake sequence off Miyagi Prefecture, located at the edge of the source area of the Tohoku-Oki earthquake was simulated. We conducted numerical simulations of earthquake generation cycles based on the rate- and state-dependent friction law representing the stress accumulation and release process on the plate interface. We also validated the results based on analyses of observational data, including time intervals and afterslip distributions for the previous Miyagi-ken-Oki earthquakes. The simulation results were then compared with repeating-earthquake-derived interplate slip observations over 30 years. The results showed that the spatial and temporal characteristics of aseismic slips on the plate interface near the  $M > 7$  Miyagi-ken-Oki source were qualitatively reproduced. The time interval between the  $M \sim 9$  earthquake and the first  $M > 7$  earthquake is shorter than the average recurrence interval of  $M > 7$  earthquakes during the latter stage of each  $M \sim 9$  earthquake cycle. In contrast, the interval between the first and the second  $M > 7$  earthquakes is the longest in each  $M \sim 9$  earthquake cycle. The time intervals of the  $M > 7$  earthquakes fluctuated in the early stage compared to those in the latter stage of the  $M \sim 9$  earthquake cycle. These characteristics were associated with the extent of the locked and afterslip areas in and around the source. Hence, monitoring the spatio-temporal distribution of the slip rate in and around the source area during the preparation process of earthquakes occurring in the downdip area off Miyagi Prefecture is very important to assess whether the next  $M > 7$  earthquake is approaching. Furthermore, earthquake cycle simulations combined with earthquake and slow slip monitoring can provide meaningful insights for long-term assessments of great interplate earthquakes.

**Keywords** Earthquake cycle, Recurrence interval, Slip deficit, Tohoku-Oki earthquake, Miyagi-ken-Oki earthquake, Repeating earthquake, Aseismic slip, Rate- and state-dependent friction law

\*Correspondence:

Ryoko Nakata

[rnakata@eps.s.u-tokyo.ac.jp](mailto:rnakata@eps.s.u-tokyo.ac.jp)

Full list of author information is available at the end of the article



© The Author(s) 2023. **Open Access** This article is licensed under a Creative Commons Attribution 4.0 International License, which permits use, sharing, adaptation, distribution and reproduction in any medium or format, as long as you give appropriate credit to the original author(s) and the source, provide a link to the Creative Commons licence, and indicate if changes were made. The images or other third party material in this article are included in the article's Creative Commons licence, unless indicated otherwise in a credit line to the material. If material is not included in the article's Creative Commons licence and your intended use is not permitted by statutory regulation or exceeds the permitted use, you will need to obtain permission directly from the copyright holder. To view a copy of this licence, visit <http://creativecommons.org/licenses/by/4.0/>.

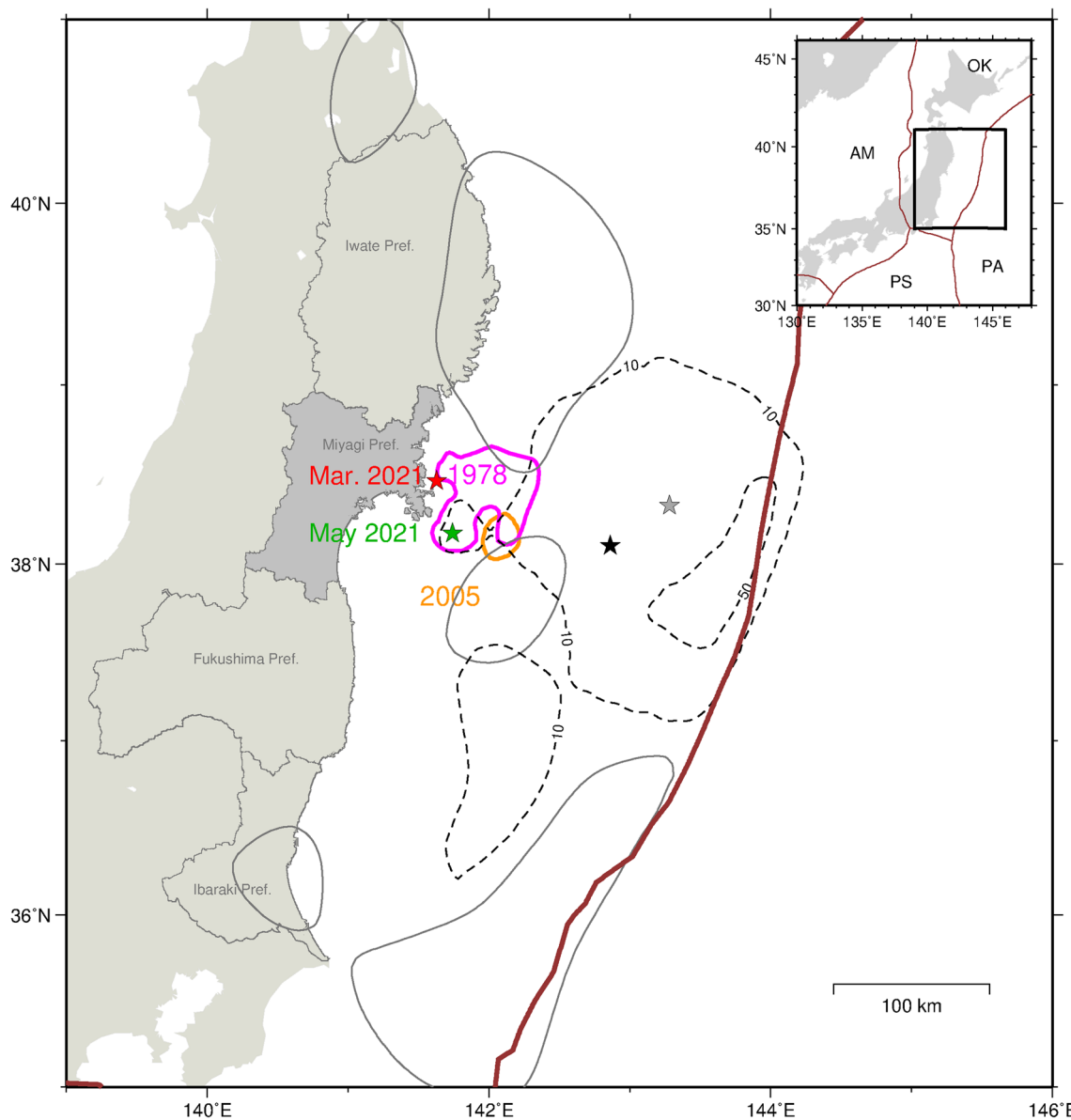


**Fig. 1** Distribution of the source areas of recent large interplate earthquakes off Miyagi prefecture and the 2011 Tohoku-Oki earthquake. Black dashed contours: coseismic slip distribution (10 and 50 m) of the 2011 Tohoku-Oki earthquake (Linuma et al. 2012). Gray lines: distribution of the estimated postseismic slip (> 0.4 m) for 0.6 years following the 2011 Tohoku-Oki earthquake (Linuma et al. 2016). Black and gray stars indicate the hypocenters of the mainshock (Mj=9.0) and foreshock (Mj=7.3) of the 2011 event, respectively, determined by JMA. The magenta and orange areas indicate the source areas (slip > 0.6 m) of the 1978 and 2005 Miyagi-ken-Oki earthquakes, respectively (Yamanaka and Kikuchi 2004; Yamanaka 2005). The red and green stars indicate the hypocenters of the March and May 2021 earthquakes determined by JMA. The gray region on land surrounded by the solid line indicates the location of Miyagi Prefecture. The brown line indicates the plate boundary (Bird 2003). The rectangle in the inset with the plate boundary (Bird 2003) represents the location of the study area. PA Pacific plate, PS Philippine Sea Plate, AM Amur plate, OK Okhotsk plate

### 1 Introduction

In the middle segment on the west side of the Japan Trench,  $M \sim 9$  and  $M > 7$  interplate earthquakes have occurred on the updip and downdip parts of the subducting Pacific Plate interface, respectively (Fig. 1). The 2011 Tohoku-Oki earthquake at  $M_j 9.0$  ( $M_j$  refers to the

magnitude determined by the Japan Meteorological Agency (JMA)) occurred on the updip side of the segment. Geological data, tsunami sediment, and historical documents indicate that the recurrence interval of great tsunamigenic earthquakes along the Japan Trench is < 1000 years (Uchida and Burgmann 2021). Whereas,

the downdip edge of the coseismic slip area in the 2011 Tohoku-Oki earthquake was located off the east coast of Miyagi Prefecture, where large (Mj7.1–7.4) earthquakes have occurred several times in the past, particularly in 1897 (M7.4) (Utsu 1979), the 1930s (1933 (Mj7.1), 1936 (Mj7.4), and 1937 (Mj7.1)), 1978 (Mj7.4), and 2005 (Mj7.2) (Headquarters for Earthquake Research Promotion 2011). The 1930s earthquakes (1933, 1936, and 1937) are treated as a single event series based on the source regions. The rupture areas of these earthquakes, which are referred to as “Miyagi-ken-Oki earthquakes,” partially overlapped, with maximum coseismic slips < 3 m (Yamanaka and Kikuchi 2004; Yamanaka 2005).

The probability of an earthquake occurring within 30 years is the most commonly used indicator for long-term evaluations provided by the Headquarters for Earthquake Research Promotion (HERP), a Japanese government organization responsible for earthquake research. The probability is calculated basically assuming a BPT (Browning Passage Time) distribution model (Matthews et al. 2002) using the occurrence time of the most recent earthquake and the mean recurrence interval of the earthquakes in the region, while Poisson process is assumed if the occurrence time of the most recent event is unknown. For the evaluation of the Miyagi-ken-Oki earthquake by HERP, the 2011 Tohoku-Oki earthquake was treated as the most recent earthquake. This is because the Tohoku-Oki earthquake ruptured a wide region including the source regions of the previous Miyagi-ken-Oki earthquakes. The slip amount of the Tohoku-Oki earthquake was estimated to be ~ 10 m in the Miyagi-ken-Oki source area (Iinuma et al. 2012) (Fig. 1), which is larger than those in previous Miyagi-ken-Oki events (Nakata et al. 2016). The mean recurrence interval was calculated to be 38.0 years using 1897, 1936, 1978, and 2011 events. The 2005 event was not used in the HERP’s evaluation because the event ruptured only a part of the previous Miyagi-ken-Oki earthquake source area (Yaginuma et al. 2007). Applying the average interval of 38.0 years and elapsed time of 10.8 years (approximate as of January 1, 2022) to the BPT distribution model, the probability of an earthquake within the next 30 years is estimated to be ~ 70–80% (HERP 2022).

Approximately 10 years after the Tohoku-Oki earthquake, Mj6.9 and 6.8 interplate earthquakes occurred in the region off Miyagi Prefecture on March 20 and May 1, 2021, respectively (Fig. 1). The coseismic slip area of the two earthquakes comprised only the western part of the source region for the 1978 Miyagi-ken-Oki earthquake (Mj7.4) (HERP 2021a, 2021b; Yoshida et al. 2022), which was one of the largest earthquakes in the Miyagi-ken-Oki segment. Although the 2021 earthquakes were smaller in magnitude than the ~ M7.4 earthquake predicted to

occur off Miyagi Prefecture (~ 70–80%) within the next 30 years by HERP, they were the largest interplate earthquakes to rupture within the 1978 source area since the 2011 Tohoku-Oki earthquake.

Nakata et al. (2016) investigated the seismicity after a great (M ~ 9) earthquake using three-dimensional numerical simulations. They suggested that the M > 7 Miyagi-ken-Oki (MYG) earthquake after the great earthquake would occur earlier than the average recurrence interval during the later stage of the interseismic period of the great earthquake. This is due to the locking conditions around the MYG patch and high-stress rate caused by the large afterslip of the M ~ 9 event at the downdip side of the M ~ 9 rupture area, promoting earthquake occurrence (Nakata et al. 2016). Although Nakata et al. (2016) have modeled five M ~ 7 earthquakes off Miyagi (MYG), off Fukushima (FKS), off Ibaraki (IBK), and at the shallow regions (SHL1 and SHL2), comparisons with observations were made qualitatively for recurrence interval and magnitude of each earthquake that occurred prior to the 2011 Tohoku-Oki earthquake.

Although Nakata et al. (2016) only focused on MYG earthquakes that occurred in the 200 years prior to an M ~ 9 earthquake and one MYG earthquake after the M ~ 9 earthquake, to reliably propose the long-term seismic activity in the MYG region, it is necessary to investigate the entire M ~ 9 earthquake cycle after knowing how well the simulation results reasonably account for recent observations. However, a long time was required to calculate multiple M ~ 9 cycles using a model with many M ~ 7 patches. Furthermore, the propagation of afterslip due to earthquakes in other areas complicates the study and description of the relationship between the MYG earthquakes and the M ~ 9 source, despite other earthquakes not being expected to significantly affect the time interval of MYG earthquakes in the earliest stage of the M9 cycle (Nakata et al. 2016). We then prepared new simulation results to discuss the recurrence interval of MYG earthquakes through the M9 earthquake cycle.

Accordingly, in this study, we examined detailed spatial and temporal characteristics of simulated slips on the plate interface off Miyagi Prefecture common to multiple great earthquake cycles obtained from one model along the Japan Trench. We then validated our findings by evaluating how well the simulation results reproduced observations since 2011. Using a similar approach as in our previous studies along the Japan Trench (Nakata et al. 2016, 2021), we numerically simulated earthquake generation cycles based on stress accumulation and release processes on the plate interface. The work in Nakata et al. (2021) is a revision of that in Nakata et al. (2016) with respect to the numerical and spatial settings of friction parameters along the trench to improve reproducibility

for the observed  $M \sim 9$  source area and long afterslip duration. Since Nakata et al. (2021) does not account for the frictional heterogeneity that represents  $M \sim 7$  earthquakes, including those of the Miyagi-ken-Oki earthquake, we performed a new calculation combining the following: the  $M \sim 9$  and Miyagi-ken-Oki earthquakes. Hence, the results of this study will improve our understanding of the basic physical processes associated with earthquake occurrence and evolution in the Miyagi-ken-Oki region throughout  $M \sim 9$  earthquake cycles.

## 2 Methods

The equations, initial conditions, basic parameters, and discretized plate geometry were the same as those used in previous studies (Nakata et al. 2016, 2021), as briefly introduced below. Details are provided in Additional file 1.

### 2.1 Numerical simulation of earthquake generation cycles

We discretized the subducting Pacific Plate interface into small planar triangular elements (Hyodo et al. 2016; Additional file 1: 1.2–1.3) and treated three triangular elements as a rectangle-like subfault (Additional file 1: Fig. S1). Seismic and aseismic events release the slip deficit accumulated during interseismic periods. The time derivative of shear stress on a rectangle-like subfault caused by slip rate changes of surrounding subfaults was evaluated by the combined effect of angular dislocations by three triangular elements within a rectangle-like subfault (Comninou and Dundurs 1975) in a homogenous elastic half-space (Hyodo et al. 2016). The quasi-dynamic model (Rice 1993) was used to treat the long cycle. We employed a rate- and state-dependent frictional law (Dieterich 1979) as an approximate mathematical model for friction behavior at the plate interface and a fault constitutive law (Nakatani 2001) to determine the interplate slip rate for a stress and strength value. We also employed an aging law (Dieterich 1979; Ruina 1983). The frictional parameters were assumed to be time-invariant in the simulations (Nakata et al. 2016, 2021).

### 2.2 Friction parameters

We assumed friction parameters  $A$ ,  $B$ , and  $L$  for each subfault (Fig. 2) based on those described by Nakata et al. (2016, 2021) to satisfy the following conditions for non-dimensional numbers  $Rb$  and  $Ru$  (Additional file 1: 1.4), which controlled the characteristics of the simulated slip (Barbot 2020). The friction parameter  $A$  ( $=a\sigma$ ) controls the slip increase rate at which the level of stress increases and reaches the strength; friction parameters  $B$  ( $=b\sigma$ ) and  $L$  control the strength recovery and slip weakening (Additional file 1: 1.1). When  $Ru > 1$ , the fault slip is unstable (Barbot 2020); however, when  $Ru \sim 1$  and  $< 1$ , the

fault slip is quasi-stable, and stable, respectively (Barbot 2020). When the  $Rb$  value is small and positive, conditions approach a neutral velocity; whereas when the  $Rb$  value is large and approaches 1, conditions correspond to a notable weakening unless  $a$  is unusually large (Barbot 2020).

The friction parameters in the aseismic background area (northern, southern, and deep segments) were the same as those described for Model B3 in Nakata et al. (2021). The  $M \sim 9$  source area assumed in the middle segment was expressed by a rectangle-like region (Nakata et al. 2021). We expressed the source area of the historical  $M > 7$  Miyagi-ken-Oki (MYG) earthquakes using a circular patch when projected onto a horizontal plane (Nakata et al. 2016). Although the spatial distribution was the same, we slightly changed the friction parameter ( $A$ ,  $B$ , and  $L$ ) values for these seismic sources from those in our previous studies (Nakata et al. 2016, 2021). In addition to  $A$ – $B$  and  $L$ , the above-mentioned nondimensional parameters are shown in Table 1. In these seismic areas,  $Ru > 1$  with a low  $Rb$ .

## 3 Results

We performed extensive numerical simulations for approximately 3300 years. Figure 3 shows the development over time of the slip deficit obtained using the model shown in Table 1 and Fig. 2. Here, we defined a slip deficit as  $V_{pl} \times \text{time} - (\text{slip at the point}) + \alpha$ , where  $V_{pl}$  is the plate convergence rate (Additional file 1: Table S1) and  $\alpha$  is a value-added for visibility and does not change with time. In Fig. 3, the slip deficit at the cross in the  $M \sim 9$  slip area (shallow middle segment in Fig. 2a) was set to zero by adjusting  $\alpha$  when the first  $M \sim 9$  earthquake of Cycle 3 occurred ( $T = 1919.3$  years). At that point, five large  $> 50$  m changes (Fig. 3a, black line) caused by  $M \sim 9$  ( $M = 8.94$ – $8.95$ ) earthquakes (such as Fig. 4a in the slip distribution) were observed, with recurrence intervals of 633–637 years. These periods between two successive  $M \sim 9$  earthquakes are hereafter referred to as “M9 earthquake cycles.”

The slip deficit at the cross in the patch labeled “MYG” in Fig. 2a was set to zero when the  $M > 7$  event immediately following the first  $M \sim 9$  earthquake of Cycle 3 occurred ( $T = 1968.7$  years in Fig. 3a). The time development of the slip deficit at the cross in the MYG patch at the downdip region of the middle segment (Fig. 3, magenta line) revealed the occurrence of numerous earthquakes with a slip of approximately 5 m. Over a period of 3300 years, earthquakes with magnitudes of 7.34–7.45 (such as those in Figs. 4b and 4c presenting the slip distributions) repeatedly occurred in the MYG patch at time intervals of 60–123 years (Figs. 3 and 5). As the source area was approximated by a single circle

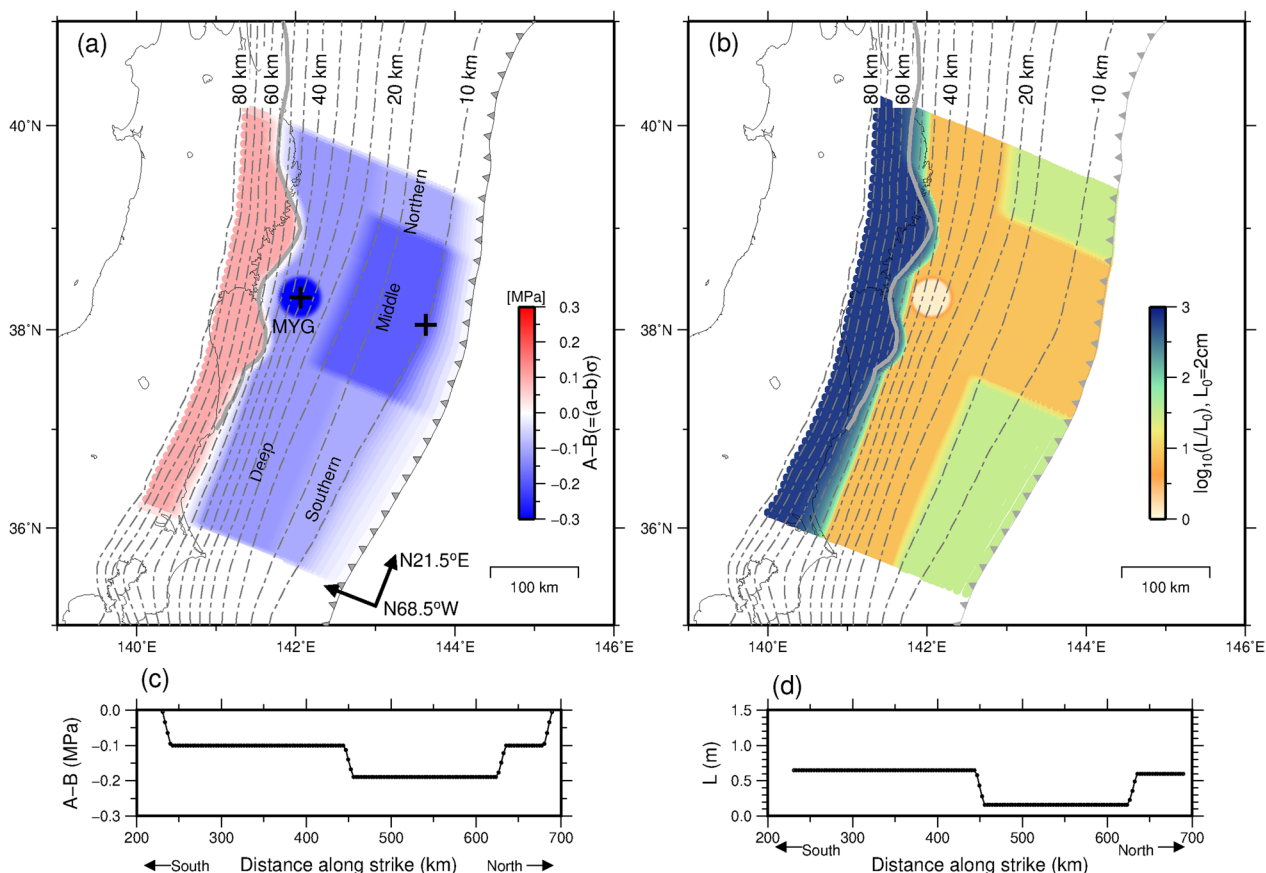


**Fig. 2** Distribution of frictional parameters used in this study. **a** Spatial distribution on the plate interface of  $(A-B)$  (MPa). Contours: depth (km) to the upper surface of the descending plate (Baba et al. 2006). Gray solid curve: downdip limit of the interplate earthquake distribution (Igarashi et al. 2001). Black crosses: locations used in Fig. 3. Barbed line: trench axis. **b** Spatial distribution of the characteristic slip distance ( $L$ ). **c-d** Profiles of  $A-B$  and  $L$  along the strike at a depth of 10.15 km. MYG, Miyagi-ken-Oki

and homogeneous frictional conditions were assumed within the circle, minimal fluctuation in the magnitude of each earthquake during the M9 earthquake cycle was expected. However, the maximum slip and magnitude of the MYG earthquakes tended to be slightly smaller immediately after the M~9 earthquake (Figs. 4c, 5e, and n) than those of the other earthquakes (Figs. 4b, 5a-c, and f-l). In addition, the coseismic slip areas of the MYG earthquakes were slightly narrower in dip direction due to a lack of slip on the updip side immediately after the M~9 earthquake (Figs. 4c and 6, red lines) when compared to those of the other MYG earthquakes (Figs. 4b and 6, blue lines), regardless of the magnitude of each MYG earthquake.

Notably, immediately after the M~9 earthquake, the resulting aseismic slip distribution after the M>7 MYG earthquake also differed from that of the other earthquakes. During the M9 earthquake cycle, aseismic slip was distributed around the patch and sometimes widely propagated to the updip (Fig. 6, light-blue lines). In

contrast, the aseismic slip did not typically propagate to the updip side immediately after the M~9 earthquake (Fig. 6, pink lines).

The recurrence intervals between MYG earthquakes showed lengthening and shortening periods during the M9 earthquake cycles. The patterns of lengthening or shortening were different in Cycles 1 to 4 in the latter half of the M9 earthquake cycle. Among them, the common characteristics were as follows. At the latest phase of each M9 earthquake cycle, the average recurrence interval of the four M>7 seismic events in the MYG patch was 69–70 years. In contrast, the variability of the recurrence interval of the MYG earthquake was large during an initial phase of the M9 earthquake cycle. The time interval between each M~9 earthquake and subsequent M>7 MYG earthquake was 49–57 years, which were shorter than the average recurrence intervals of the MYG earthquakes during each M9 earthquake cycle. Furthermore, the next MYG event had the longest interval from the previous one (>100 years).

**Table 1** Parameters at the northern, middle, southern, and deep segments and the MYG patch

Segments	Parameters	Values	Sources/Segments	Parameters	Values
Northern	A-B (MPa)	-0.10	MYG	A-B (MPa)	-0.320
	b-a	0.0020		b-a	0.0064
	L (m)	0.60		L (m)	0.026
	Rb=(b-a)/b	0.118		Rb=(b-a)/b	0.299
	Ru	0.271		Ru	14.2
	Length (km)*2	65 (*1)		Radius (km)	23
Middle	A-B (MPa)	-0.19	Deep (≤ 62 km *3)	A-B (MPa)	-0.12
	b-a	0.0038		b-a	0.0024
	L (m)	0.16		L (m)	0.15
	Rb=(b-a)/b	0.202		Rb=(b-a)/b	0.138
	Ru	5.047		Ru	9.6
	Length (km)*2	170		Length (km)*2	480
Southern	A-B (MPa)	-0.10	Deep (> 62 km *3)	A-B (MPa)	0.10
	b-a	0.0020		b-a	-0.0020
	L (m)	0.65		L (m)	13.0
	Rb=(b-a)/b	0.118			
	Ru	0.865			
	Length (km)*2	225 (*1)		Length (km)*2	480

\* 1: Transition between the middle segment and northern/southern segment is 10 km

\* 2: Length along strike direction

\* 3: Changes depending on the down-dip limit of the interplate earthquake distribution (Igarashi et al. 2001)

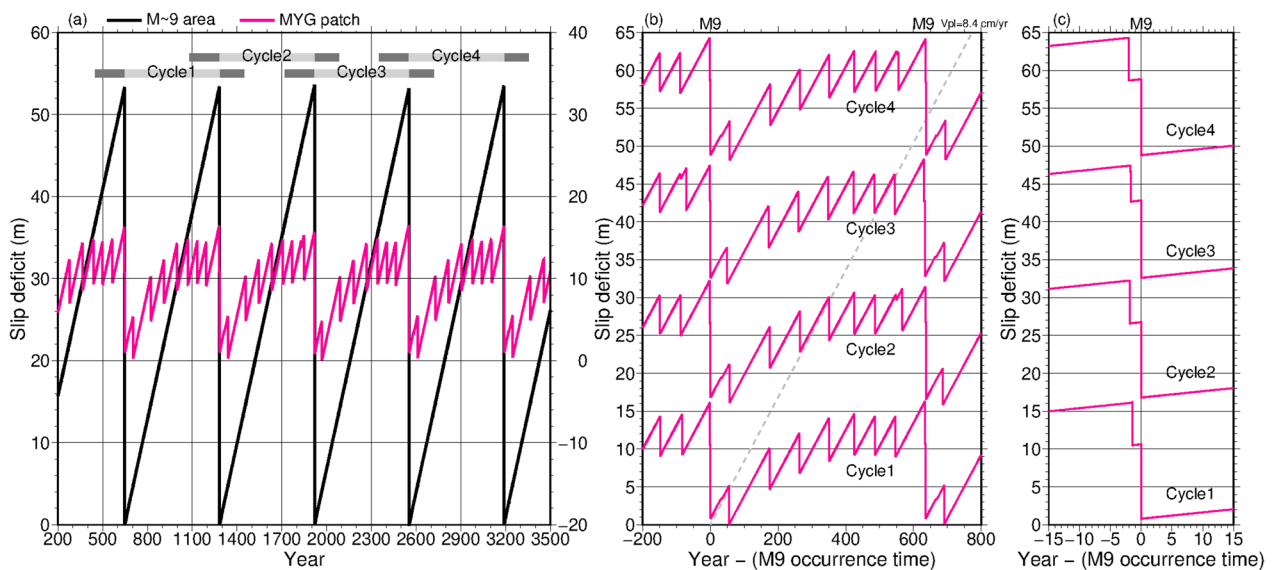


**Fig. 3** Temporal distribution of slip deficits obtained using the friction model shown in Fig. 2. **a** Temporal distribution of simulated slip deficits over a 3300-year period at a point within the M~9 source area (black) and Miyagi-ken-Oki (MYG) source area (magenta) at the locations of the crosses shown in Fig. 2. Cycles 1~4 (light gray lines) represent a period from one M~9 earthquake to the next M~9 earthquake. The slip deficit in the M~9 area was set to zero when the first M~9 earthquake of Cycle 3 occurred ( $T = 1919.3$  years), and the vertical axis is on the left. The slip deficit at the MYG area was set to zero when the MYG earthquake occurred immediately after the first M~9 earthquake of Cycle 3 ( $T = 1968.7$  years), and the vertical axis is on the right. **b** Temporal distribution of the simulated slip deficit at the cross in the MYG patch shown in Fig. 2a for a 1000-year period from 200 years before the occurrence time of each M~9 earthquake in Cycles 1~4. The time when the slip deficit is zero differs from that in (a), and the slip deficit is a relative value for ease of viewing. The period combines the dark and light gray lines in (a). Horizontal axis ( $T'$ ): 0 years at the time of the M~9 earthquake, which is the start of each cycle. **c** Enlarged diagram of (b) for  $T' = -15$  to 15 years

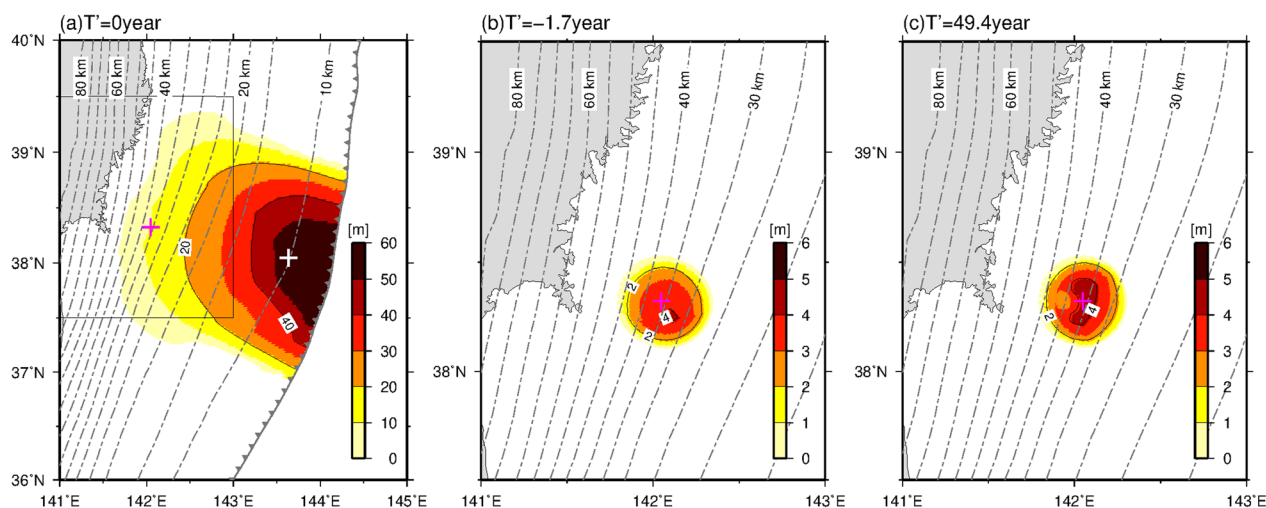


**Fig. 4** Coseismic slip distribution obtained using the friction model shown in Fig. 2. **a** Simulated coseismic slip distribution of the  $M=8.95$  earthquake that occurred at  $T'=0$  years in Cycle 3. Magenta and white crosses: locations used in Fig. 3. The large square surrounding the magenta cross indicates the area described in (b) and (c). **b** Simulated coseismic slip distribution for one of the events in the Miyagi-ken-Oki (MYG) patch in the last stage of the  $M\sim 9$  earthquake cycle, the  $M=7.34$  earthquake at  $T'=-1.7$  years in Cycle 3. Magenta cross: location used in Fig. 3. **c** Simulated coseismic slip distribution for one of the first events after an  $M\sim 9$  earthquake, the  $M=7.35$  earthquake at  $T'=49.4$  years in Cycle 3

At the end of each  $M9$  earthquake cycle, the interval between the last MYG earthquake and  $M\sim 9$  earthquake was 0.8–2.1 years (Fig. 3c), which was much shorter than the average recurrence interval of the MYG events; on the other hand, the interval and magnitude of earthquakes occurring in the MYG patch at the final stage of each  $M9$  earthquake cycle varied between cycles. These characteristics were common to all cycles over the evaluated 3300-year period (Fig. 3b). Although a small slow slip event occurred near the MYG patch towards the end of Cycle 2 ( $\sim 550$  years in Fig. 3b), this phenomenon did not affect the overall recurrence interval and aseismic slip distribution trends.

#### 4 Discussion

During an  $M\sim 9$  earthquake cycle, the stress and strain at the plate boundary vary spatiotemporally, and these continuous variations are expected to cause changes in the time interval of MYG earthquakes. In other words, changes in recurrence intervals of MYG earthquakes may reflect such changes in physical conditions. In this section, we divided an  $M\sim 9$  earthquake cycle into three stages and extracted characteristics common to all  $M\sim 9$  earthquake cycles: from an  $M\sim 9$  earthquake to the subsequent MYG earthquake (Stage I: earliest stage), from the first MYG to the next MYG earthquake (Stage II: early stage), and from the second MYG to the next  $M\sim 9$  earthquake (Stage III: later stage). We first compared the simulation results with observational studies to assess the validity of the simulations. We then identified factors influencing the recurrence intervals of  $M>7$

earthquakes at each stage. To this end, the results were examined using multiple patch models with other  $M\sim 7$  earthquakes at the updip and southern regions and the corresponding stage to the post-2021 earthquakes off Miyagi among the three stages. Finally, we presented several important points for the long-term evaluation of  $M>7$  earthquakes off Miyagi Prefecture.

##### 4.1 Comparison between observations and simulations

Based on more than 110 years of observations since 1897, the variability in the recurrence intervals of the Miyagi-ken-Oki earthquakes has been relatively small. In the simulation, at the later stage of the  $M9$  earthquake cycle (Stage III), the average of the recurrence intervals for the  $M>7$  events in the MYG patch was relatively constant. At the end of each  $M9$  earthquake cycle, however, the interval between the last MYG event and the next  $M\sim 9$  earthquake in the simulations was significantly shorter than the observed interval between the 1978 and 2011 events.

The interval between the 2005 Miyagi-ken-Oki earthquake and the 2011 Tohoku-Oki earthquake, on the other hand, was much shorter than the observed average recurrence interval of Miyagi-ken-Oki earthquakes. This short interval may be related to the extremely short time between the last MYG earthquake and the next  $M\sim 9$  event in each  $M9$  earthquake cycle obtained in the simulations. Afterslip of the last MYG earthquake might have facilitated the occurrence of the subsequent  $M\sim 9$  earthquake, as suggested for the 2005 Miyagi-ken-Oki earthquake (Suito et al. 2011; Ozawa et al. 2012). If so, it may have significant implications for predicting the

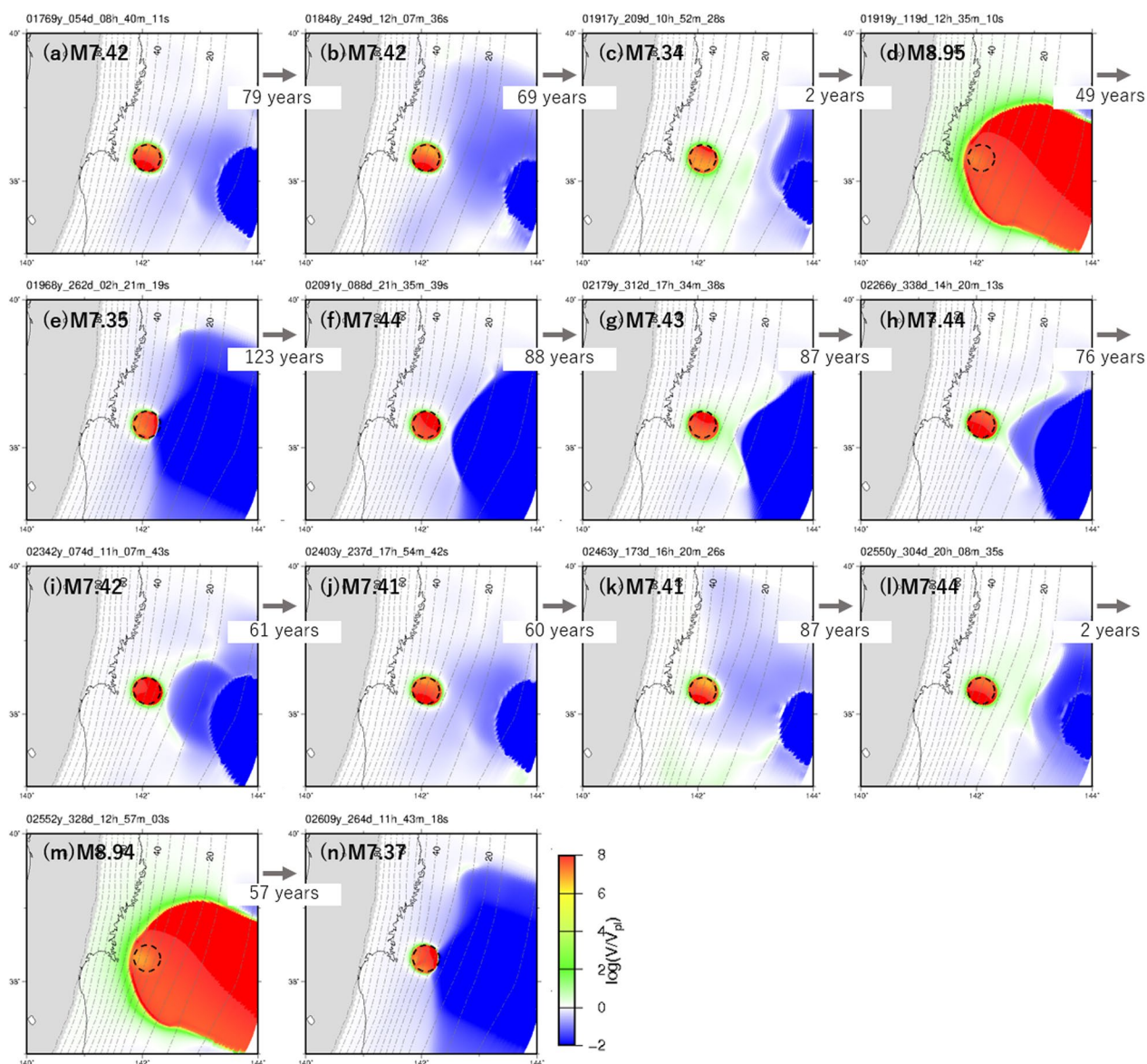


**Fig. 5** Snapshots of the simulated slip velocity distribution during Cycle 3 shown in Fig. 3. **a–c**  $M > 7$  earthquake in the Miyagi-ken-Oki (MYG) patch. Slip velocity is normalized to the plate convergence rate,  $V_{pl}$ . The time interval between adjacent panels is shown below the arrow between the panels. **d** and **m**  $M \sim 9$  earthquakes that occurred within a time interval of 633 years. **e–l, n**  $M > 7$  earthquakes that repeatedly occurred in the MYG patch. Blue and red areas indicate the locked parts and unstable slipping parts of the fault, respectively. Yellow/green and white indicate slow slip and plate convergence rates, respectively

occurrence of great interplate earthquakes, but we will not go into this issue further in this study.

Differences in slip distribution described by the simulations in this study were consistent with the observations from past earthquakes. Widely distributed aseismic slips during Stage III were consistent with the observed aseismic slips of the 2005 and 1978 earthquakes. The aseismic slip extending to the updip side was evidenced by the onshore geodetic observation

(Miura et al. 2007) and the increased activity of repeating earthquakes (Uchida et al. 2006, 2007) after the 2005 earthquake. Although geodetic observations only detected the deep aseismic slip after the 1978 earthquake, Uchida et al. (2006) and Hino et al. (2007) pointed out remarkable similarity between the aftershock distributions of the 1978 and 2005 earthquakes on the updip side of the mainshock ruptures. The 2005 aftershocks included repeating earthquakes, suggesting

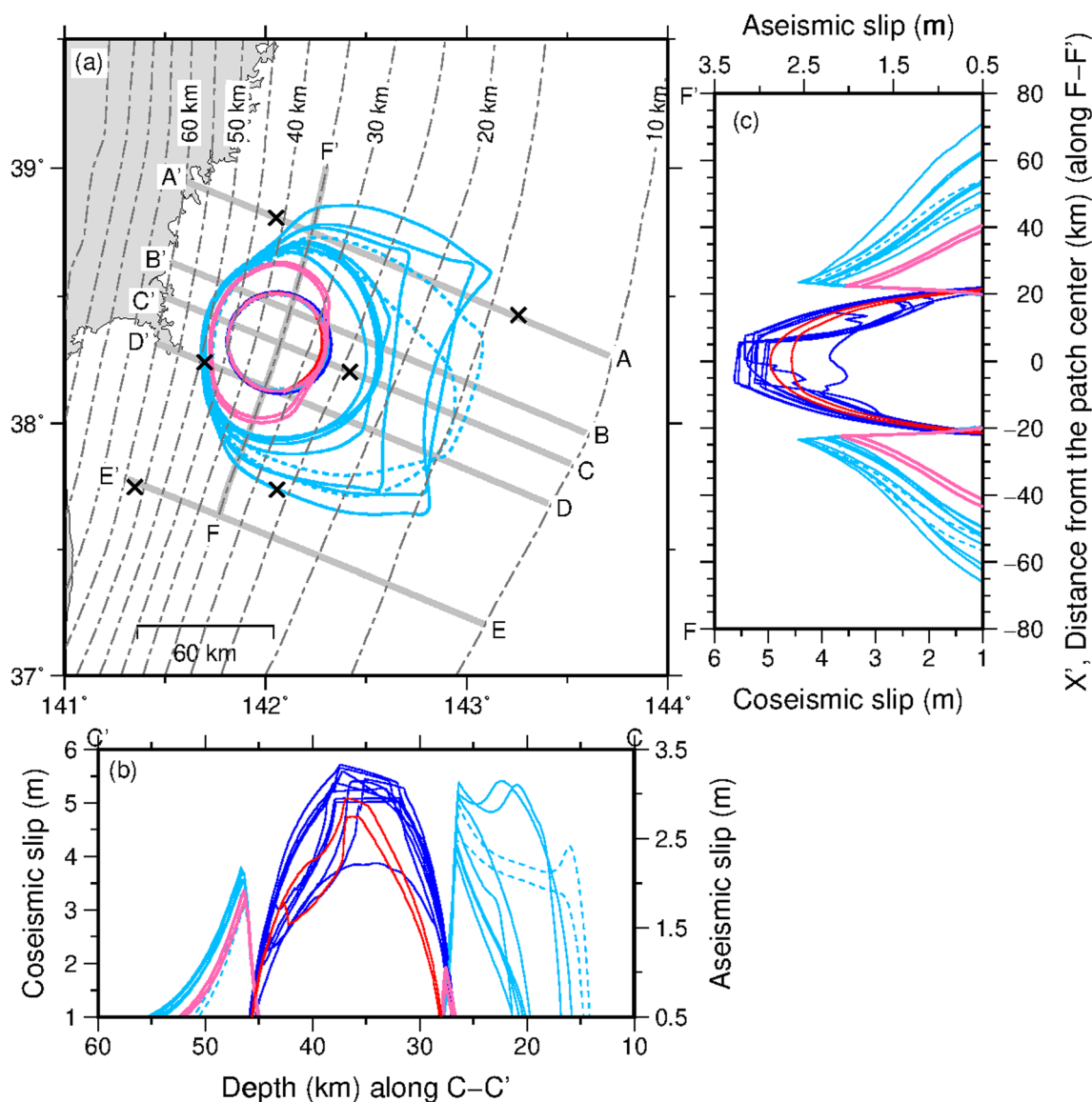


**Fig. 6** Coseismic and aseismic slip distributions of  $M > 7$  earthquakes around the Miyagi-ken-Oki (MYG) patch. Coseismic slip is extracted when slip velocity ( $V$ )  $> 1$  cm/year. Aseismic slip is the slip remaining after removing coseismic slip from cumulative slip over the three years from the rupture initiation time of each  $M > 7$  earthquake. **a** Map view of simulated coseismic slip ( $> 1$  m) and aseismic slip ( $> 1$  m) distributions of the MYG earthquakes shown in Fig. 5. The coseismic slip of the MYG earthquakes before the  $M \sim 9$  earthquake (10 events; Fig. 5a–c, f–l) is indicated in blue, and light-blue lines show the aseismic slip following these earthquakes. Among the light-blue lines, the dotted lines indicate events that occurred just before  $M \sim 9$  earthquakes with only one year of cumulative slip (Fig. 5c and l). The reason for the one-year duration is owing to the shortest time interval of  $< 3$  years between the MYG earthquake and  $M \sim 9$  earthquake. The coseismic slip of the MYG earthquakes after the  $M \sim 9$  earthquake (2 events; Fig. 5e and n) is indicated in red, and pink lines show the aseismic slip following these MYG earthquakes. Black crosses represent the points shown in Fig. 7. **b** and **c** Slip profiles of coseismic slip and aseismic slip distributions of the MYG earthquakes shown in Fig. 5 along gray lines (C–C', across the MYG patch center; F–F', along 35 km depth) in the map panel

that the shallow 1978 aftershocks were due to aseismic slip as observed in the 2005 activity. The slightly narrower coseismic slip distributions simulated in Stage I could be considered similar to those of the 2021 earthquakes (Yoshida et al. 2022), which ruptured exclusively on the downdip side of the rupture areas of  $M$  earthquakes

in 1978 (Yamanaka and Kikuchi 2004) and the 1930s (Umino et al. 2007).

To perform comparisons with observations of small to medium earthquakes, which could not be addressed in this simulation, cumulative slips are shown (Fig. 7). The development over time of the averaged cumulative

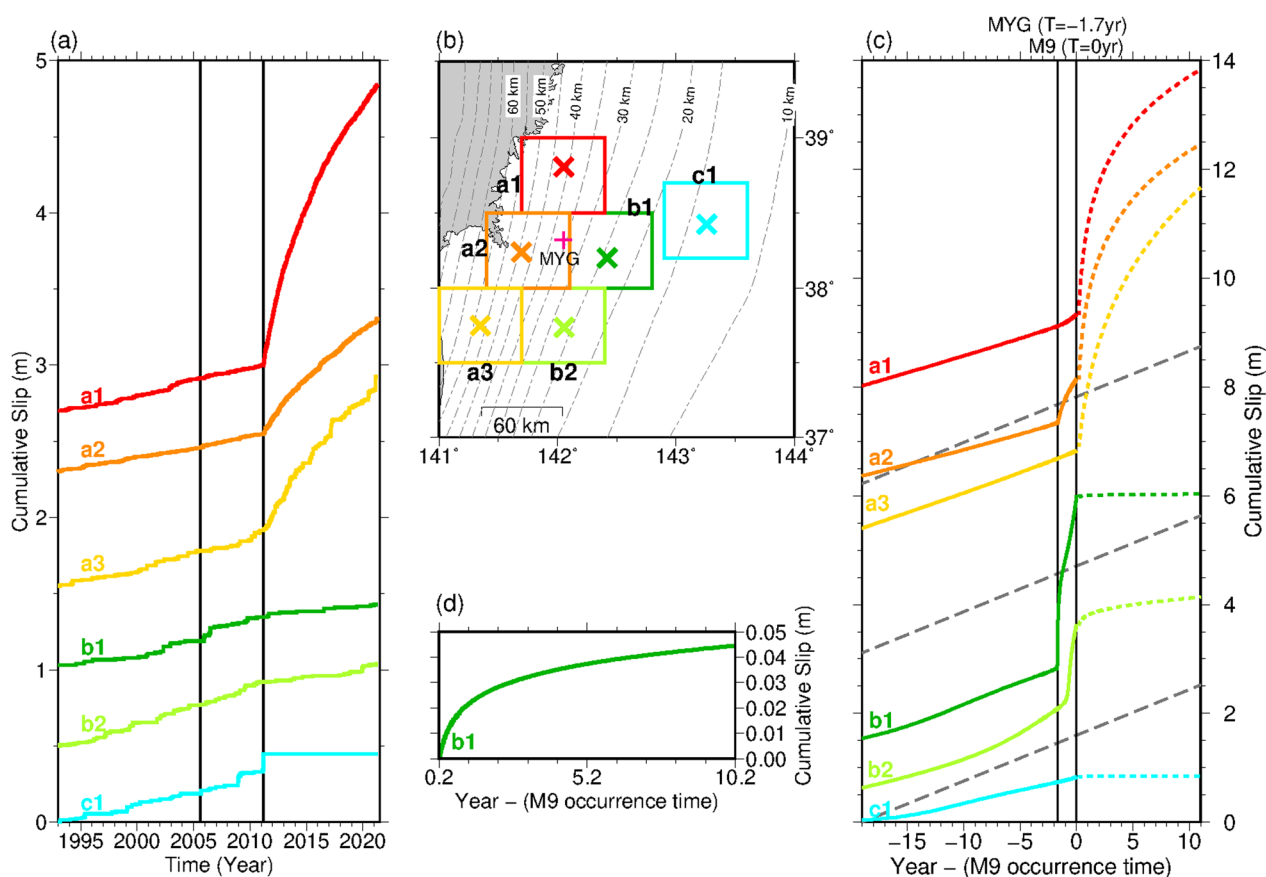


**Fig. 7** Cumulative slip in the middle segment before and after an M~9 earthquake. **a** Cumulative slip from 1993–2021 estimated from observed repeating earthquake groups within each rectangle. Vertical line: time of 2005 off Miyagi and 2011 Tohoku-Oki earthquakes. **b** Location of each rectangle. Crosses: locations shown in (c). **c** Simulated cumulative slip time series over 30 years (from  $T' = -19$  years to  $T' = 11$  years) in Cycle 3. Points at crosses in regions a1, a2, a3, b1, b2, and c1 shown in (b) were used. The behavior within each rectangle was represented by the points marked with crosses. Solid lines: from  $T' = -19$  to 0 years. Dotted lines: from  $T' = 0.2$  to 11 years by subtracting the slip due to the M~9 earthquake. The horizontal axis ( $T'$ ): 0 years at the time of the M~9 earthquake. Dashed gray lines: slope at  $V_{pi}$ . Vertical lines: time of M > 7 and M~9 earthquakes. **d** Enlarged view of (c) at point b1. MYG, Miyagi-ken-Oki

interplate slip estimated from repeating earthquakes (Uchida and Matsuzawa 2013) exhibited a heterogeneous pattern. As of 2021, the curves could be categorized into three groups: regions showing large slip after the Tohoku-Oki earthquake (group a; a1, a2, and a3 in Fig. 7a–b), small slip after the earthquake (group b; b1 and b2), and no postseismic slip (group c; c1). Moreover, following the Tohoku-Oki earthquake, many repeating earthquakes emerged on the downdip side that were aseismic before the Tohoku-Oki earthquake while interplate earthquakes were relatively absent from inside the Tohoku-Oki rupture area (Yoshida et al. 2022). The former corresponded to group a, while the latter corresponded to group c. Similar results were observed for the simulation after an M~9 earthquake. That is, immediately after an M~9 earthquake (Stage I), a large afterslip on the deeper side off Miyagi Prefecture (a1, a2, and a3 in Fig. 7c) was reproduced. Furthermore, a small aseismic

slip occurred between the area off Miyagi Prefecture and the M~9 area (b1 and b2 in Fig. 7c and d). A point on the updip side (c1 in Fig. 7c) became nearly locked, which is reasonable given that c1 is located within the unstable area ruptured in the M~9 earthquake (Additional file 2: Fig. S2.1). Although the amount of slip varied, after an M~9 earthquake, the slip on the updip side (b1, b2, and c1) was sufficiently small compared to that on the downdip side (a1, a2, and a3). These results were consistent with prior observations (Fig. 7a).

Observations of repeating earthquakes showed a small increase in slip in area b1 after the 2005 earthquake (M7.2), with no change detected in area a2 (Fig. 7a). In contrast, geodetic data revealed a small afterslip around the a2 area (Miura et al. 2007). In the simulation results (Figs. 6a and 7c), the slips clearly increased at points a2, b1, and b2 after the MYG earthquake (M7.34) that occurred ~1.7 years before the M~9 earthquake.

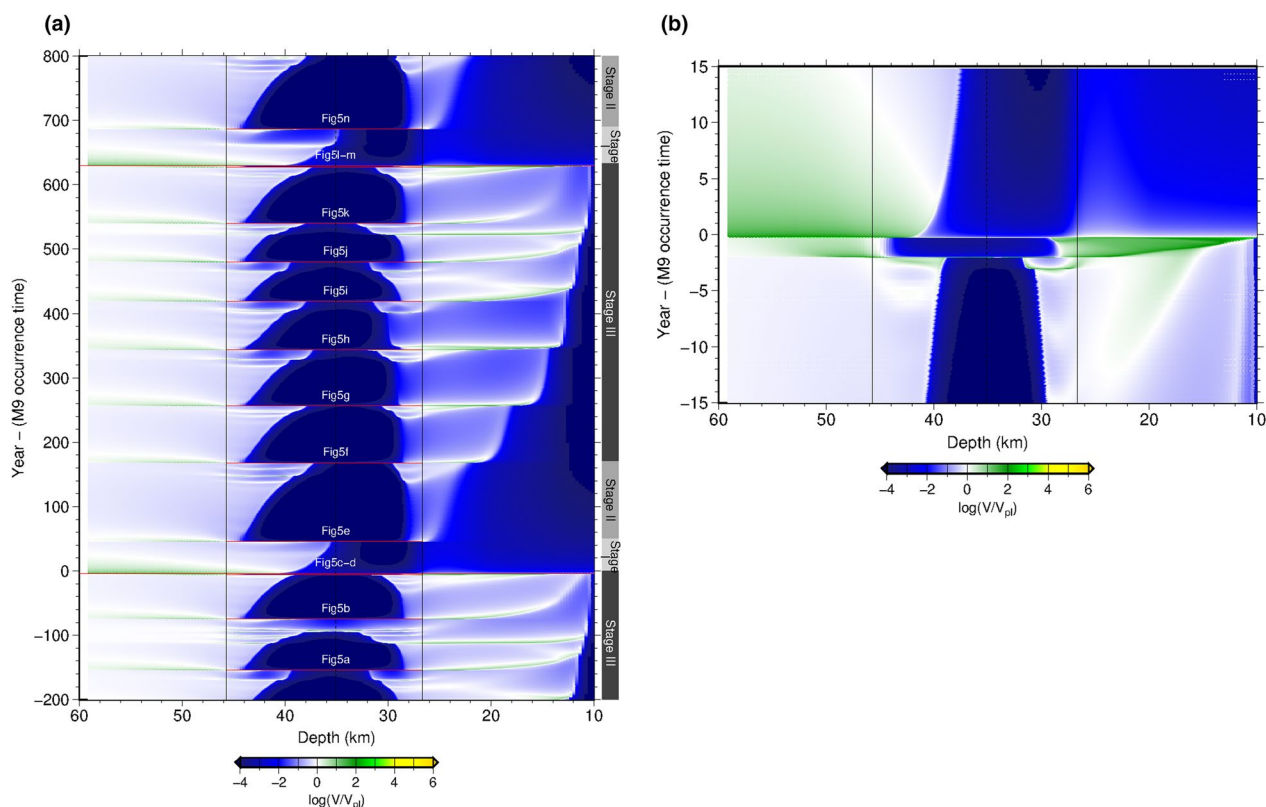


**Fig. 8** **a** Time development of simulated slip velocity during Cycle 3. Horizontal axis: depth (km) through the approximate center of the Miyagi-ken-Oki (MYG) patch (along the C–C' line). Vertical axis: 0 years at the time of the first M~9 earthquake during Cycle 3 (similar to Fig. 3). Red horizontal lines: timing of M > 7 or M~9 earthquakes shown in Fig. 5. Black dashed line: center of the MYG patch; solid vertical lines: a radius of 23 km from the center of MYG patch. **b** Enlarged diagram of **(a)** for  $T' = -15$  to 15 years

The amount of simulated aseismic slips was larger than that in the observations. However, the estimated moment during 2.72 years for the postseismic slip of the 2005 earthquake ( $12.19 \times 10^{19}$  Nm in Suito et al. 2011) was comparable with the three-year aseismic slip estimated at the later stage of the M9 cycle in the simulation ( $8.7$ – $11.6 \times 10^{19}$  Nm). Therefore, the simulation reproduced the overall seismicity features in the Miyagi-ken-Oki region, although the simulation and observations sometimes differed with respect to factors such as the time intervals between each earthquake and aseismic slip amounts.

#### 4.2 Factors influencing recurrence intervals of M > 7 Miyagi-ken-Oki earthquakes

In Sect. 4.1, we showed that the simulation results in this study were sufficiently reasonable to describe the difference in the spatiotemporal behavior of slips (both seismic and aseismic) before and after an M~9 earthquake when compared to prior observations. Although the descriptions might not be sufficient, they provide a necessary comparison to validate our simulation results. Therefore,

we investigated the physical process responsible for the differences in the recurrence intervals among the three stages.

The trend in the time evolution of the slip deficit in the center of the MYG patch (Fig. 3, magenta line) was variable throughout an M9 earthquake cycle. More specifically, although the change in the slip deficit was large in Stages I and II, the change in the slip deficit was relatively low and nearly constant in Stage III as the next M~9 earthquake approached. We then compared the spatial and temporal changes in slip velocity and stress within and around the MYG patch, along dip and strike directions in each stage (Figs. 8 and 9, Additional file 2: Figs. S2.2–S2.5).

During Stage III ( $\sim T' = -200$ – $0$  and  $170$ – $630$  years in Fig. 8), immediately after each MYG earthquake, the slip velocity within the patch became low (locked condition) and the afterslip was distributed both in the updip and downdip direction around the patch. The locked area within the patch (Fig. 8 and Additional file 2: Figs. S2.3–S2.4) gradually narrowed from the outer edge of the patch toward the center as the next M > 7 earthquake

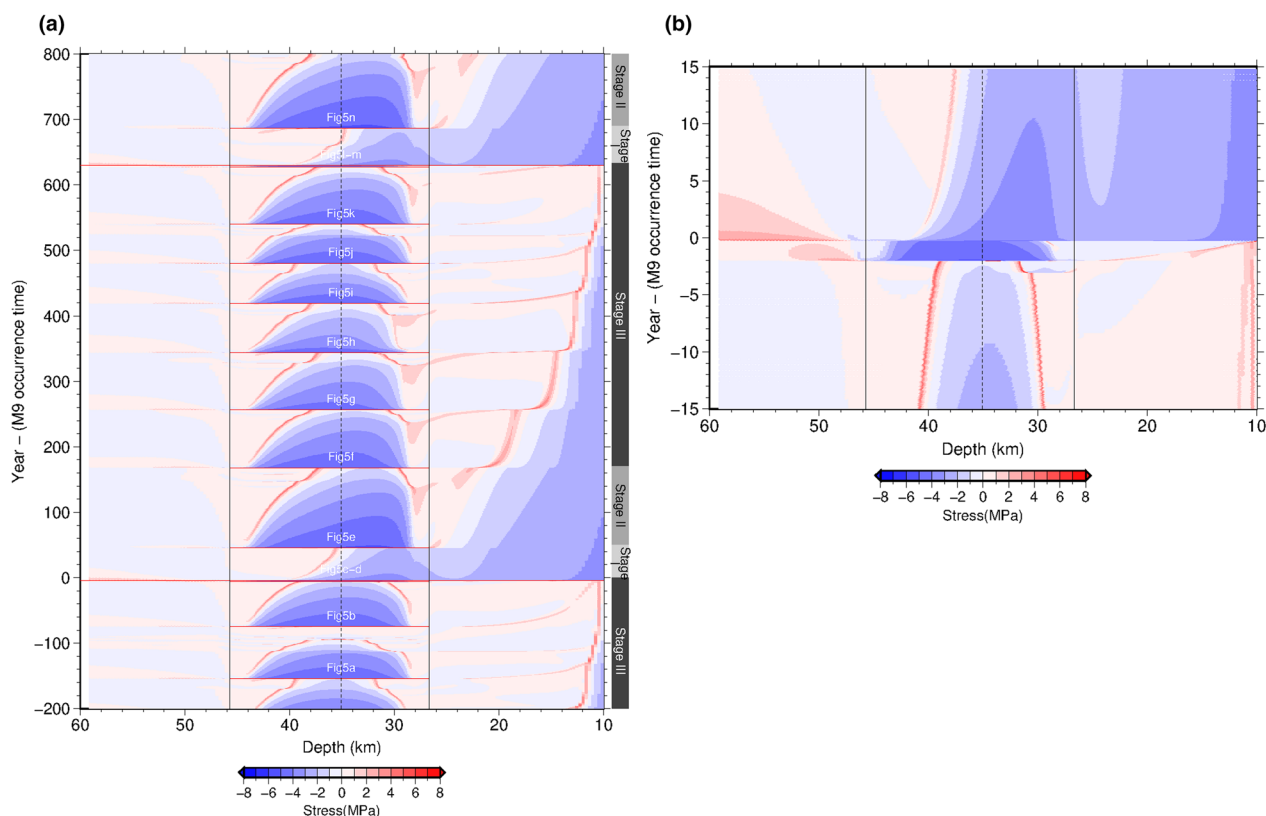


**Fig. 9** **a** Time development of simulated stress during Cycle 3. Horizontal axis: depth (km) through the approximate center of the Miyagi-ken-Oki (MYG) patch (along the C–C' line). Vertical axis: 0 years at the time of the first M~9 earthquake during Cycle 3 (similar to Fig. 3). Red horizontal lines: timing of M > 7 or M~9 earthquakes shown in Fig. 5. Black dashed line: center of the MYG patch; solid vertical lines: a radius of 23 km from the center of MYG patch. **b** Enlarged diagram of **(a)** for  $T' = -15$  to 15 years

approached, whereas, the center of the patch remained locked. Eventually, the inside of the patch became unstable, slow slip occurred around the edges within the patch, and fast slip (i.e., an earthquake) occurred later.

The difference in the slip distribution and recurrence interval between Stage I ( $\sim T' = 0-50$  and 630–690 years in Fig. 8) and the other stages might be attributed to the wide distribution of the locking area due to the M~9 earthquake. After an M~9 earthquake, due to the strong locking of the updip side of the MYG patch (Figs. 5e, 5n, and 8), the afterslip following the first MYG earthquake did not propagate substantially to the updip side (Figs. 6 and 8). The afterslip following an M~9 earthquake showed a higher slip velocity (Nakata et al. 2016) and longer duration only on the downdip side than in the other stages. In addition, the afterslip penetrated inside the patch, and the locked area within the patch was narrower than in the other stages. The stress level in the strongly locked patch was higher in Stage I than in the other stages (Fig. 9). Finally, the first MYG earthquake occurred earlier due to the high stress accumulation rate (Nakata et al. 2016).

During Stage II ( $\sim T' = 50-170$  years in Fig. 8), the locking on the downdip side of the patch was similar to that in Stage III. Given that the afterslip area was especially narrow and weak on the updip side of the MYG patch, the locked area on the updip edge (approximately 27 km depth) remained wider than in Stage III. On the updip side of the locked area within the patch, it subsequently narrowed more slowly than that in Stage III. Stress in the patch remained low during the early period of Stage II (Fig. 9). Therefore, the next M > 7 earthquake will occur following a longer time interval than that in Stage III, as the interior of the patch will remain relatively stable for a longer period.

In numerical simulations using a two-dimensional rheological model at the Japan Trench (Barbot 2020), M~7 earthquakes occurred with a recurrence interval that increased during an M~9 earthquake cycle. Simply stated, the recurrence interval was longer in the later part of the M9 earthquake cycle than in the beginning. This simple situation can be considered similar to this study, where Stage I has a shorter recurrence interval than Stage III. However, the behavior at the area between the M~9

large slip area and  $M \sim 7$  earthquake during Stages I and II differed from the current results. More specifically, in the current study simulation, this area was locked, or an exceptionally small slip occurred between the areas (Figs. 7 and 8). In contrast, in the simulations conducted by Barbot (2020), the area between the  $M_w \sim 9$  large slip area and  $M \sim 7$  earthquake continued to creep even after an  $M \sim 9$  earthquake. In addition, our study showed a gradual narrowing of the locked area during Stage II (Fig. 8), whereas Barbot (2020) reported continual creep as in Stage I. This discrepancy is likely due to differences in model settings between this study and Barbot (2020). Barbot (2020) modeled the lower arc between the forearc basement and the mantle wedge as a permanent structural boundary with a velocity-strengthening condition. The assumption of a velocity-strengthening boundary allows  $M \sim 7$  interplate earthquakes to frequently occur and always creep during interseismic periods, even after a giant rupture. In addition, the locked region within the  $M \sim 9$  source area did not change during an interseismic period of an  $M \sim 9$  earthquake cycle. That is, the physical processes that shorten the time interval of MYG earthquakes differed between our results showing three stages and those of Barbot (2020) without Stage II. If the rate at which the locked area shrunk is faster than the simulation, a large afterslip would have occurred at the updip area following the earthquake at the end of Stage I. The locked area would then largely disappear. In that case, Stage I would be followed by Stage III. Seismic and geodetic observations on the updip side are important to know if Stage II is present.

#### 4.3 Multiple patch model with other $M \sim 7$ earthquakes

In the previous section, for simplicity, a circular unstable patch was located only in the Miyagi-ken-Oki segment. In reality, however,  $M \sim 7$  earthquakes have been observed on the updip side and, in some cases, occurred after the Miyagi-ken-Oki earthquake (e.g., the earthquakes in 2005 and 2011, 1978 and 1981, and the 1930s and 1939). We also conducted numerical simulations using other models, which included seismic patches that assumed the same radius at the same location as SHL1 and SHL2 in the middle segment used in Nakata et al. (2016). One of these is shown in Additional file 2: Fig. S2.6 and Table S2. This model is the same as that in Fig. 2 and Table 1, except for the SHL1 and SHL2 patches.

We performed numerical simulations for a period of  $\sim 2700$  years. The results showed a similar trend to that in the model with only the MYG patch concerning the spatiotemporal distribution of the  $M \sim 9$  and MYG area was also obtained in the model with two additional patches. In the shallow part, the time development for the slip deficit showed four  $M \sim 9$  earthquakes ( $M = 8.97$ ,

8.95, 8.91, and 8.97) with 638, 553, and 643 years between them, respectively (Additional file 2: Fig. S2.7). Earthquakes of  $M = 7.26\text{--}7.50$  frequently occurred in the MYG patch with time intervals of 50–136 years. As reported in Sect. 3, even with this model, the time evolution of the slip deficit in the center of the MYG patch (Additional file 2: Fig. S2.7) was not constant throughout an  $M_9$  earthquake cycle. The slip deficit rate was large after the  $M \sim 9$  earthquake but became low and constant as the next  $M \sim 9$  earthquake approached. The intervals between each great earthquake and the subsequent  $M > 7$  earthquake in the MYG patch were 28–56 years; these were the shortest intervals during each  $M_9$  earthquake cycle. Furthermore, the next MYG earthquake had the longest interval from the previous one ( $> 100$  years). At the latest stage of the  $M_9$  earthquake cycle, the average recurrence intervals of the four  $M > 7$  earthquakes in the MYG patch were 71–74 years. At the end of the  $M_9$  earthquake cycle, the interval between the MYG and great earthquakes was 0.7–5.5 years in this model. The time interval between the  $M = 7.43$  earthquake in the MYG patch and the second  $M \sim 9$  earthquake ( $T = 1295$  years, Cycle 2) was 5.5 years, consistent with the observations (5.5 years between the  $M 7.1$  earthquake in 2005 and  $M 9.0$  mainshock).

At the SHL1 patch, two to three earthquakes of  $M = 6.81\text{--}7.43$  occurred during an  $M_9$  earthquake cycle. At the SHL2 patch, zero to two  $M < 7$  earthquakes occurred during an  $M_9$  earthquake cycle. The time interval between the  $M = 7.43$  earthquake in the SHL1 patch and the first  $M \sim 9$  earthquake ( $T = 657$  years, Cycle 1) was 55 h, consistent with observations from March 2011 (51 h between the  $M 7.3$  foreshock and  $M 9.0$  mainshock). The time interval and magnitude of the earthquakes that occurred in the MYG and SHL1 patches in the final stage of the  $M_9$  earthquake cycle differed between cycles. The time interval of each event just prior to an  $M \sim 9$  earthquake did not affect the behavior after the  $M \sim 9$  earthquake.

Characteristics for the slip deficit rate (Additional file 2: Fig. S2.7), coseismic/afterslip distributions of the  $M > 7$  MYG earthquake (Additional file 2: Fig. S2.8), and cumulative slip distributions (Additional file 2: Fig. S2.9) were similar to those in the one-patch model. A notable difference was that the aseismic slip (afterslip of an MYG earthquake) that propagated to the east sometimes triggered another  $M > 7$  and  $M \sim 7$  earthquake at the SHL1 and/or SHL2 patches within the  $M \sim 9$  source, respectively (Additional file 2: Fig. S2.8). In the present simulations, there was also a case of an SHL1 earthquake triggering an MYG earthquake. Thus, it is reasonable to discuss characteristics common to all cycles concerning MYG earthquakes based on the model without SHL1 and SHL2 patches.

In addition, we showed other models, which included seismic patches that assumed the same radius at the same location as FKS and IBK in the southern segment used in the study by Nakata et al. (2016). Frictional parameters and temporal distribution of slip deficits are shown in Additional file 2: Figs. S2.10, S2.11, and Table S3. This model is the same as that in Fig. 2 and Table 1, except for the SHL1, SHL2, FKS, and IBK patches. Spatial and temporal development of the slip deficit at the MYG patch showed similar characteristics as the simple model.

#### 4.4 March and May 2021 earthquakes

Next, we examined whether the 2021  $M < 7$  earthquakes that occurred in the earliest stage of the great earthquake cycle caused the transition from Stage I to II, or whether Stage I continued. No  $M > 7$  earthquakes have occurred in the region since 2011. As the source area was approximated using a single and homogeneous circle, we did not model  $M < 7$  earthquakes similar to those in 2021 in the MYG area. The 2021 earthquakes can simply be regarded as small earthquakes that cannot be reproduced during Stage I by this model.

The epicenters of the 2021 earthquakes were located at almost the exact site of the epicenter of the 1937 earthquake (Umino et al. 2007). In the later stage of the  $M \sim 9$  earthquake cycle ending with the 2011 Tohoku-Oki earthquake, the source area migrated from updip to downdip in the order of 1933 (Mj7.1), 1936 (Mj7.4), and 1937 (Mj7.1) (Umino et al. 2007). In contrast, after the 2021 earthquakes, seismic activity between the March and May source areas suggested that the afterslip of the 2011 great earthquake continued in this area (Yoshida et al. 2022). Thus, the western part of the 1978 source does not appear to have fully locked after the 2021 earthquakes. Otherwise, the eastern part of the 1978 source possibility remained locked. These situations differed from the beginning of Stage II in our simulation in that the whole MYG patch is locked. In addition, the interplate earthquakes indicated that the aseismic slip at the downdip side of the MYG patch was still larger than before 2011 (Fig. 7a; Yoshida et al. 2022).

Therefore, the current situation is still considered to be in the early-to-mid phase of Stage I. This suggests that the remaining areas of the 1978 source that had not ruptured in 2021 might rupture at the end of the remaining short Stage I. Observing the spatial and temporal changes in aseismic slips after the 2021 earthquakes in the eastern region are necessary to investigate the possibility of future earthquakes in the eastern region of the 1978 earthquake rupture area (also those in the 1930s). It is also important to determine whether the Tohoku-Oki afterslip on the downdip side has continued. For more realistic simulation results, we will adopt a multiscale

circular patch model (Ide and Aochi 2013) to reproduce a partial rupture in the MYG region, such as in the 1930s, 2005, and 2021 earthquakes.

#### 4.5 Possibility of an $M > 7$ earthquake off Miyagi within the next 30 years

The slips and average recurrence intervals of the simulated MYG earthquakes were larger and longer than those observed. As discussed in Sect. 4.2, we concluded that the spatial relationship of slip and/or locked area between the  $M9$  earthquake and the MYG earthquakes is significant in constraining the length of the recurrence intervals. We next sought to examine the possibility of an  $M > 7$  earthquake occurring off Miyagi within the next 30 years based on our simulations. We would not show probability (%) as HERP has presented because we do not consider providing a percentage is the only direct way to evaluate the long-term activity. Similar to Nakata et al. (2016), the present results showed that “the time interval between the  $M \sim 9$  earthquake and subsequent  $M > 7$  MYG earthquake was shorter than the average recurrence time interval during the later stage of the  $M9$  earthquake cycle.” This might have been caused by stress accumulation between the locked area at the updip side and the large afterslip at the downdip side within and around the MYG patch.

If a large amount of afterslip following an  $M \sim 9$  earthquake occurred surrounding the MYG patch, it could create a similar situation to that in Stage III. In that case, the time interval of the  $M > 7$  MYG earthquake would be relatively constant throughout the  $M \sim 9$  cycle. However, this hypothesis was rejected given that the aseismic slip observed after the 2011 Tohoku-Oki earthquake was sufficiently smaller on the updip side of the MYG patch than that on the downdip side (Fig. 7a).

Nakata et al. (2016) also presented several scenarios in which the interval between an  $M \sim 9$  earthquake and a subsequent  $M > 7$  MYG earthquake is longer than the average interval of several MYG earthquakes during the later stage of the  $M9$  earthquake cycle. A large slow slip occurred in those scenarios instead of an  $M > 7$  earthquake. The 2021 earthquakes differed from a simulated slow slip in terms of slip velocity. Thus, scenarios with a longer time interval than the average recurrence interval after an  $M \sim 9$  earthquake would be rejected. Hence, scenarios with a shorter time interval than the average recurrence interval are still possible. Given that the current situation is considered to be in Stage I, an earthquake larger than those in 2021 will likely occur shortly.

These simulations showed that the variation in recurrence intervals within Stage III is small compared to the changes from Stage I to Stage II and Stage II to Stage III. Therefore, it can be concluded that the recurrence

interval of MYG earthquakes in the later stage of an M9 earthquake cycle is stable. Therefore, in the later stage, it is reasonable to rely on the history of the several past earthquakes regarding long-term evaluation, as HERP had done prior to 2011. In contrast, in the earliest stage of the M9 earthquake cycle, long-term evaluation based on the recent history is unsuitable because of exceptional situations based on the occurrence of the great earthquake. In this case, the long-term (30 years) evaluation should refer to the spatiotemporal behavior of aseismic slips in and around the MYG source in addition to the past recurrence intervals.

## 5 Conclusions

Using numerical simulations, we investigated the spatiotemporal distribution of interplate slip velocity for the  $M > 7$  Miyagi-ken-Oki earthquake during an  $M \sim 9$  earthquake cycle along the Japan Trench. Despite approximating the  $M > 7$  source area with a single circle, the simulation results were validated in terms of observed characteristics of relatively constant time intervals for the  $M > 7$  Miyagi-ken-Oki earthquakes before the 2011 Tohoku-Oki earthquake, afterslip distributions of the  $M > 7$  Miyagi-ken-Oki earthquakes in 1978 and 2005, coseismic slip distributions for the 2021 earthquakes located in the western region of the primary rupture areas of the earthquakes in 1978, and repeating-earthquake-derived interplate slip observations before and after the 2011 Tohoku-Oki earthquake. These observations were qualitatively consistent with the simulations before and after  $M \sim 9$  earthquakes. Moreover, we reported that the recurrence intervals of the Miyagi-ken-Oki earthquakes varied in the early and later stages of the  $M \sim 9$  earthquake cycle. These differences might be related to the extent of the locked and afterslip areas in, and around, the Miyagi-ken-Oki source, particularly on the updip side. Although the simulation results were not exactly the same as the observations with respect to the time interval of earthquakes and aseismic slip amounts, based on our simulations, the recurrence interval of the Miyagi-ken-Oki earthquake was unstable during the early stage after the  $M \sim 9$  earthquake. For this period, observations of aseismic slip and seismicity in and around the expected sources are important to assess the timing of expected Miyagi-ken-Oki earthquakes and long-term probability evaluations based on past recurrence intervals.

### Abbreviations

M	Magnitude
Mj	Magnitude as determined by the Japan Meteorological Agency
JMA	Japan Meteorological Agency
MYG	Miyagi-ken-Oki
HERP	Headquarters for Earthquake Research Promotion
BPT	Brownian Passage Time

## Supplementary Information

The online version contains supplementary material available at <https://doi.org/10.1186/s40645-023-00566-y>.

**Additional file 1. 1.1-1.3.** Detailed description of Methods. **Table S1.**

Parameters used in this study. **Figure S1.** Schematic illustration of the definition of subfaults.

**Additional file 2.** Additional Figures and Tables. **Figure S2.1.** Position of the squares used in Figure 7. **Figures S2.2-2.5.** Time development of simulated slip velocity during Cycle 3. **Figure S2.6.** Distribution of frictional parameters for three patches. **Figure S2.7.** Temporal distribution of slip deficits obtained using the friction model shown in Figure S2.6. **Figure S2.8.** Time development of simulated slip velocity obtained using the friction model shown in Figure S2.6. **Figure S2.9.** Cumulative slip in the middle segment before and after an  $M \sim 9$  earthquake obtained using the friction model shown in Figure S2.6. **Figure S2.10.** Distribution of frictional parameters for five patches. **Figure S2.11.** Temporal distribution of slip deficits obtained using the friction model shown in Figure S2.10. **Table S2.** Parameters for the northern, middle, southern, and deep segments and the MYG, SHL1, and SHL2 patches shown in Figure S2.6. **Table S3.** Parameters for the FKS and IBK patches shown in Figure S2.10.

### Acknowledgements

The computational resources of the Earth Simulator provided by JAMSTEC and the Cyberscience Center, Tohoku University, were used for all numerical simulations. Figures were drawn using Generic Mapping Tools (Wessel and Smith 1998). We would like to thank T. Matsuzawa, an associated editor, and three reviewers for their thoughtful suggestions and insights. We would also like to thank Editage ([www.editage.com](http://www.editage.com)) for English language editing.

### Author contributions

RN performed the numerical simulations, proposed the topic, and conceived and designed the study. NU helped in the preparation and interpretation of the observation data. TH assisted with the preparation and interpretation of the simulation results and collaborated with the corresponding author in the construction of the manuscript. RH helped validate the simulation results based on the observational data and collaborated with the corresponding author in the construction of the manuscript. All authors read and approved the final manuscript.

### Funding

This work was supported by JSPS KAKENHI (Grant Numbers JP21K04604, JP19H05596, JP21K03713, and JP21H05206).

### Availability of data and material

The datasets generated and/or analyzed during the current study are not publicly available because of the large size of the datasets; however, the data are available from the corresponding author on reasonable request.

### Declarations

#### Competing interests

The authors declare that they have no competing interests.

#### Author details

<sup>1</sup>Graduate School of Science, The University of Tokyo, 7-3-1 Hongo, Bunkyo-Ku, Tokyo 113-0033, Japan. <sup>2</sup>Graduate School of Science, Tohoku University, 6-6, Aramaki-Aza-Aoba, Aoba-Ku, Sendai 980-8578, Japan. <sup>3</sup>Earthquake Research Institute, The University of Tokyo, 1-1-1 Yayoi, Bunkyo-Ku, Tokyo 113-0032, Japan. <sup>4</sup>Research and Development Center for Earthquake and Tsunami Forecasting (FEAT), Research Institute for Marine Geodynamics (IMG), Japan Agency for Marine-Earth Science and Technology (JAMSTEC), 3173-25 Showa-Machi, Kanazawa-Ku, Yokohama 236-0001, Japan.

Received: 29 September 2022 Accepted: 29 June 2023

Published online: 04 July 2023

## References

- Baba T, Ito A, Kaneda Y, Hayakawa T, Furumura T (2006) 3-D seismic wave velocity structures in the Nankai and Japan Trench subduction zones derived from marine seismic surveys. Abstract S111–006 presented at the JpGU Meeting 2006, Makuhari, Japan, 14–18 May 2006. [https://www2.jpgu.org/meeting/2006/pdf/S111/S111-006\\_e.pdf](https://www2.jpgu.org/meeting/2006/pdf/S111/S111-006_e.pdf). Accessed 1 July 2022.
- Barbot S (2020) Frictional and structural controls of seismic super-cycles at the Japan trench. *Earth Planets Space* 72:63. <https://doi.org/10.1186/s40623-020-01185-3>
- Bird P (2003) An updated digital model of plate boundaries. *Geochem Geophys Geosyst* 4:1027. <https://doi.org/10.1029/2001GC000252>
- Comninou M, Dundurs J (1975) The angular dislocation in a half space. *J Elast* 5:203–216. <https://doi.org/10.1007/BF00126985>
- Dieterich JH (1979) Modeling of rock friction: 1. Experimental results and constitutive equations. *J Geophys Res* 84:2161–2168. <https://doi.org/10.1029/JB084iB05p02161>
- Headquarters for Earthquake Research Promotion (2011) Evaluations of occurrence potentials of subduction-zone earthquakes. [http://www.jishin.go.jp/evaluation/long\\_term\\_evaluation/subduction\\_fault/](http://www.jishin.go.jp/evaluation/long_term_evaluation/subduction_fault/). (Japanese). Accessed 1 July 2022.
- Headquarters for Earthquake Research Promotion (2021a) Evaluation of earthquake offshore Miyagi Prefecture on March 20, 2021a. [https://www.jishin.go.jp/main/chousa/21apr\\_miyagi/index-e.htm](https://www.jishin.go.jp/main/chousa/21apr_miyagi/index-e.htm). Accessed 1 July 2022.
- Headquarters for Earthquake Research Promotion (2021b) Evaluation of seismic activities for May 2021b. <https://www.jishin.go.jp/main/chousa/21jun/index-e.htm>. Accessed 1 July 2022.
- Headquarters for Earthquake Research Promotion (2022) Evaluation of occurrence potentials of subduction-zone earthquakes. <https://www.jishin.go.jp/main/choukihyoka/ichiran.pdf>. Accessed 1 July 2022.
- Hino R, Suzuki K, Yamamoto Y, Nishino M, Kanazawa T, Yamada T, Nakahigashi K, Mochizuki K, Shinohara M, Kuwano A, Aoki G, Tanaka M, Araki E, Kodaira S, Fujie G, Kaneda Y (2007) Aftershock distribution of the 2005 Miyagi-oki earthquake ( $M 7.2$ ) revealed by ocean bottom seismological observation: preliminary results. *Zisin* 2(59):297–308. <https://doi.org/10.4294/zisin.59.297>
- Hyodo M, Hori T, Kaneda Y (2016) A possible scenario for earlier occurrence of the next Nankai earthquake due to triggering by an earthquake at Hyuga-nada, off southwest Japan. *Earth Planets Space* 68(6):1–17. <https://doi.org/10.1186/s40623-016-0384-6>
- Ide S, Aochi H (2013) Historical seismicity and dynamic rupture process of the 2011 Tohoku-Oki earthquake. *Tectonophysics* 600:1–13. <https://doi.org/10.1016/j.tecto.2012.10.018>
- Igarashi T, Matsuzawa T, Umino N, Hasegawa A (2001) Spatial distribution of focal mechanisms for interplate and intraplate earthquakes associated with the subducting Pacific plate beneath the northeastern Japan arc: a triple-planed deep seismic zone. *J Geophys Res* 106:2177–2191. <https://doi.org/10.1029/2000JB900386>
- Iinuma T, Hino R, Kido M, Inazu D, Osada Y, Ito Y, Ohzono M, Tsushima H, Suzuki S, Fujimoto H, Miura S (2012) Coseismic slip distribution of the 2011 off the Pacific Coast of Tohoku Earthquake ( $M 9.0$ ) refined by means of seafloor geodetic data. *J Geophys Res*. <https://doi.org/10.1029/2012JG009186>
- Iinuma T, Hino R, Uchida N, Nakamura W, Kido M, Osada Y, Miura S (2016) Seafloor observations indicate spatial separation of coseismic and postseismic slips in the 2011 Tohoku earthquake. *Nat Commun* 7:13506. <https://doi.org/10.1038/ncomms13506>
- Miura S, Iinuma T, Yui S, Sato T, Tachibana K, Hasegawa A (2007) Interplate slip distribution inferred from co- and post-seismic deformation associated with the 2005 Miyagi-oki earthquake ( $M 7.2$ ). *Zisin* 2(59):371–379. <https://doi.org/10.4294/zisin.59.371>
- Matthews MV, Ellsworth WL, Reasenber PA (2002) A Brownian model for recurrent earthquakes. *Bull Seismol Soc Am* 92:2233–2250. <https://doi.org/10.1785/0120010267>
- Nakata R, Hori T, Hyodo M, Ariyoshi K (2016) Possible scenarios for occurrence of  $M \sim 7$  interplate earthquakes prior to and following the 2011 Tohoku-Oki earthquake based on numerical simulation. *Sci Rep* 6:25704. <https://doi.org/10.1038/srep25704>
- Nakata R, Hori T, Miura S, Hino R (2021) Presence of interplate channel layer controls of slip during and after the 2011 Tohoku-Oki earthquake through the frictional characteristics. *Sci Rep* 11:6480. <https://doi.org/10.1038/s41598-021-86020-9>
- Nakatani M (2001) Conceptual and physical clarification of rate and state friction: Frictional sliding as a thermally activated rheology. *J Geophys Res* 106:13347–13380. <https://doi.org/10.1029/2000JB900453>
- Ozawa S, Nishimura T, Munekane H, Suito H, Kobayashi T, Tobita M, Imakiire T (2012) Preceding, coseismic, and postseismic slips of the 2011 Tohoku earthquake Japan. *J Geophys Res*. <https://doi.org/10.1029/2011JB009120>
- Rice JR (1993) Spatio-temporal complexity of slip on a fault. *J Geophys Res* 98:9885–9907. <https://doi.org/10.1029/93JB00191>
- Ruina A (1983) Slip instability and state variable friction laws. *J Geophys Res* 88:10359–10370. <https://doi.org/10.1029/JB088iB12p10359>
- Suito H, Nishimura T, Tobita M, Imakiire T, Ozawa S (2011) Interplate fault slip along the Japan Trench before the occurrence of the 2011 off the Pacific coast of Tohoku Earthquake as inferred from GPS data. *Earth Planets Space* 63:615–619
- Uchida N, Bürgmann R (2021) A decade of lessons learned from the 2011 Tohoku-Oki earthquake. *Rev Geophys*. <https://doi.org/10.1029/2020RG000713>
- Uchida N, Matsuzawa T (2013) Pre- and postseismic slow slip surrounding the 2011 Tohoku-oki earthquake rupture. *Earth Planet Sci Lett* 374:81–91. <https://doi.org/10.1016/j.epsl.2013.05.021>
- Uchida N, Matsuzawa T, Hirahara S, Hasegawa A (2006) Small repeating earthquakes and interplate creep around the 2005 Miyagi-oki earthquake ( $M = 7.2$ ). *Earth Planets Space* 58:1577–1580
- Uchida N, Matsuzawa T, Miura S, Hirahara S, Hasegawa A (2007) Interplate quasi-static slip off Miyagi and Fukushima Prefectures estimated from small repeating earthquake data. *Zisin* 2(59):287–295
- Umino N, Kono T, Okada T, Nakajima J, Matsuzawa T, Uchida N, Hasegawa A, Tamura Y, Aoki G (2007) Relocation of the  $M \sim 7$  Miyagi-oki earthquakes in the 1930s: Seismic slips of asperities that were re-ruptured during the 1978  $M 7.4$  Miyagi-oki earthquake? *Zisin* 2(59):325–337. <https://doi.org/10.4294/zisin.59.325>
- Utsu T (1979) Seismicity of Japan from 185 through 1925—a New Catalog of Earthquakes of  $M > 6$  Felt in Japan and smaller earthquakes which caused damage in Japan-. *Bull Earthq Res Inst* 54:253–308
- Wessel P, Smith WHF (1998) New, improved version of generic mapping tools released. *Eos Trans Am Geophys Union* 79:579. <https://doi.org/10.1029/98EO00426>
- Yaginuma T, Okada T, Hasegawa A, Kato K, Takemura M, Yagi Y (2007) Coseismic slip distribution of the 2005 Miyagi-Oki ( $M 7.2$ ) earthquake estimated by inversion of strong-motion and teleseismic waveforms—Its relation with the 1978 Miyagi-Oki earthquake ( $M 7.4$ ). *Zisin* 2(60):43–53. <https://doi.org/10.4294/zisin.60.43>
- Yamanaka Y (2005) EIC Seismological\_Note. No.168. [https://www.eic.eri.u-tokyo.ac.jp/sanchu/Seismo\\_Note/2005/EIC168.html](https://www.eic.eri.u-tokyo.ac.jp/sanchu/Seismo_Note/2005/EIC168.html). Accessed 1 July 2022.
- Yamanaka Y, Kikuchi M (2004) Asperity map along the subduction zone in northeastern Japan inferred from regional seismic data. *J Geophys Res*. <https://doi.org/10.1029/2003JB002683>
- Yoshida K, Matsuzawa T, Uchida N (2022) The 2021  $Mw 7.0$  and  $Mw 6.7$  Miyagi-Oki earthquakes nucleated in a deep seismic/aseismic transition zone: possible effects of transient instability due to the 2011 Tohoku earthquake. *J Geophys Res* 127:202. <https://doi.org/10.1029/2022JB024887>

## Publisher's Note

Springer Nature remains neutral with regard to jurisdictional claims in published maps and institutional affiliations.